CrossMark

Modelling volumetric growth in a thick walled fibre reinforced artery

T.S.E. Eriksson [a,*], P.N. Watton [b,c], X.Y. Luo [d], Y. Ventikos [e]

[a] Department of Engineering Science, Institute of Biomedical Engineering, University of Oxford, UK
[b] Department of Computer Science, University of Sheffield, UK
[c] INSIGNEO Institute for in silico Medicine, University of Sheffield, UK
[d] School of Mathematics and Statistics, University of Glasgow, UK
[e] Department of Mechanical Engineering, University College London, UK

ARTICLE INFO

ABSTRACT

A novel framework for simulating growth and remodelling (G&R) of a fibre-reinforced artery, including volumetric adaption, is proposed. We show how to implement this model into a finite element framework and propose and examine two underlying assumptions for modelling growth, namely *constant individual density* (CID) or *adaptive individual density* (AID). Moreover, we formulate a novel approach which utilises a combination of both AID and CID to simulate volumetric G&R for a tissue composed of several different constituents. We consider a special case of the G&R of an artery subjected to prescribed elastin degradation and we theorise on the assumptions and suitability of CID, AID and the mixed approach for modelling arterial biology. For simulating the volumetric changes that occur during aneurysm enlargement, we observe that it is advantageous to describe the growth of collagen using CID whilst it is preferable to model the atrophy of elastin using AID.

© 2014 The Authors. Published by Elsevier Ltd. This is an open access article under the CC BY license (http://creativecommons.org/licenses/by/3.0/).

1. Introduction

The focus of this paper is to develop concepts for simulating the volumetric changes that occur to a fibre reinforced composite soft-tissue such as arteries as a consequence of growth and remodelling (G&R) of the constituents. Most prior works on arterial G&R utilised either conceptual geometries, membrane formulations or simplified axisymmetric motions, see, e.g., the works by Gleason and Humphrey (2005), Baek et al. (2006), Eriksson et al. (2009), Watton and Hill (2009), Watton et al. (2011a), Valentín et al. (2011) to name a few. These works have all contributed to set the foundation, and provide novel insights for arterial G&R. However, in a fairly recent review article by Humphrey and Holzapfel (2012), the need for more advanced patient-specific computational models is discussed. For these types of models to become reality, there is a need to handle arbitrary geometries and thick-walled and volume changing materials. Steps toward this goal have been made in recent papers by, e.g., Schmid et al. (2012) and Valentín et al. (2013), where volumetric changes in finite element simulation of simple cubes, as well as a general three dimensional (3-D) framework for G&R of an axisymmetric

* Corresponding author. Tel.: +46 70 260 7885.
  E-mail address: thomas@tseeriksson.se (T.S.E. Eriksson).

cylinder, have been shown. Here, we use an existing model for arterial G&R as a basis (Watton et al., 2004), extending it to a thick-walled, 3-D and volume changing model and discuss the implications of fundamental assumptions about the growth process.

First, we briefly outline the structure, biology and mechanical model of the arterial wall. Arteries consist of three layers, the intima, the media and the adventitia, going from inner to outer layer. For a healthy artery, the main structural constituents are elastin fibres and vascular smooth muscle cells (VSMCs), mostly found in the media, and collagen fibres found in the media and the adventitia. The components are embedded in a ground substance, which is a hydrophilic gel rich in proteoglycans, Wagenseil and Mecham (2009). Following the approach by Holzapfel et al. (2000) on arterial modelling, we neglect the influence of the intimal layer, which under young and healthy conditions bears almost no load, as well as the active mechanical contribution from the VSMCs. Hence, we only model the passive vascular response.

During the progression of many vascular diseases, such as cerebral aneurysm or abdominal aortic aneurysm, the dilation of an artery is associated with a significant loss of the elastin constituent (He and Roach, 1994). Simultaneously, the collagen fabric adapts (via G&R) to compensate for the loss of load borne by the elastinous constituents and the changes to the geometry. Collagen growth relates to changes in the total mass of collagen whereas collagen remodelling relates to changes in the natural reference configurations that the fibres are recruited to load bearing. In general, it is assumed that collagen fibres, which are in a continual state of deposition and degradation, are configured to the artery in the loaded configuration in a small state of stretch. Consequently, as the geometry of the artery changes the reference configurations of the fibres evolve. As presented in Section 2, we follow the G&R approach proposed by Watton et al. (2004), but follow Schmid et al. (2010, 2013) and extend the formulation to a thick-walled model of the arterial wall which incorporate non-volume changing (isochoric) measures as well as an invariant basis. Moreover, we propose and implement a novel approach for modelling volumetric growth and remodelling (VGR) for a mixture of constituents.

A recent study by Valentín et al. (2013) showed as a special case for verification that a pressurised cylindrical model of an artery (consisting of elastin only) will decrease in radius if elastin mass degradation is simulated by enforcing (isotropic) volumetric loss. This is, perhaps, counter intuitive of what one would expect to happen to a mature artery which is subject to elastin degradation or fragmentation. Consequently, the numerical approach to simulate elastin degradation when using a computational framework which can simulate volumetric adaption may need careful attention. In this study, we propose a novel formulation to model the volumetric changes that occur to the arterial wall as a consequence of local changes in mass of constituents. Mass changes can be implemented by changes in density (with fixed volume) or changes in volume (with fixed density) or a combination of the two. We observe that whether the artery shrinks or enlarges depends on which assumption for constituent growth is used, i.e. constant individual density (CID) or adaptive individual density (AID); CID means that the density of a given constituent in a material does not change when its mass is increased or decreased; AID means that the volume of a constituent remains constant when its mass is altered. We will detail these approaches in Section 2, where we define the model components used for VGR of a fibre composite, here specialised for an artery. In Section 3 we show numerical examples illustrating the main features of the model and how it can be applied on AAA evolution. We discuss the proposed model and the underlying biological assumptions in Section 4 followed by some concluding remarks in Section 5.

2. Material and methods

The model of the arterial wall simulates the instantaneous mechanical response due to applied loading and the long-term mechanical response due to G&R of constituents. Consequently, it is convenient to employ two separate time scales: one short time scale, t in seconds, for mechanical equilibrium where the material is assumed to be incompressible and one long time scale, τ in years, for G&R. The kinematics needed and used in this paper are outlined in Section 2.1 and a strain-energy function used for describing the individual mechanical responses of the constituents relative to their natural reference configuration of an artery is shown in Section 2.2. A volumetric function that is used in a penalty scheme to enforce the volume changes is shown in Section 2.3 followed by the material and spatial stress tensors in Section 2.4. Section 2.5 is then devoted to the development of the VGR formulations including mass, density and volumetric changes.

2.1. Kinematics

Using the deformation gradient $\mathbf{F}$, the right and left Cauchy–Green tensors are $\mathbf{C} = \mathbf{F}^T\mathbf{F}$ and $\mathbf{b} = \mathbf{F}\mathbf{F}^T$, respectively. In the short time scale, which governs mechanical equilibrium, the volume ratio (or Jacobian determinant) between $dV(t_0)$, where t_0 is the time in the reference configuration, and $dV(t)$, where t is the time in the current configuration, is given by $J(t) = dV(t)/dV(t_0)$ or equivalently $J(t) = \det \mathbf{F} > 0$. An isochoric deformation gradient, $\overline{\mathbf{F}}$, originating from Flory (1961), is obtained from defining

$$\mathbf{F} \equiv (J^{1/3}\mathbf{I})\overline{\mathbf{F}} \quad \text{where} \quad \overline{\mathbf{F}} = J^{-1/3}\mathbf{F} \text{ leading to } \det \overline{\mathbf{F}} = 1. \tag{1}$$

The modified (isochoric) right and left Cauchy–Green tensors are now $\overline{\mathbf{C}} = \overline{\mathbf{F}}^T\overline{\mathbf{F}} = J^{-2/3}\mathbf{C}$ and $\overline{\mathbf{b}} = \overline{\mathbf{F}}\overline{\mathbf{F}}^T = J^{-2/3}\mathbf{b}$, respectively. Isochoric material invariants are further constructed as $\bar{I}_1 = \overline{\mathbf{C}}:\mathbf{I}$, $\bar{I}_2 = 1/2(\bar{I}_1^2 - \overline{\mathbf{C}}^2:\mathbf{I})$ and $\bar{I}_3 = \det(\overline{\mathbf{C}}) = 1$, where $\mathbf{I}$ is the second order identity tensor. For an anisotropic material, with two fibre families ($i = 1, 2$) in the Lagrangian directions $\mathbf{a}_{0,i}$, we may

further construct the additional isochoric pseudo-invariants $\bar{I}_{4,i} = \overline{\mathbf{C}} : \mathbf{A}_{0,i} = \bar{\lambda}_i^2$ and $\bar{I}_{5,i} = \overline{\mathbf{C}}^2 : \mathbf{A}_{0,i}$, where $\mathbf{A}_{0,i} = \mathbf{a}_{0,i} \otimes \mathbf{a}_{0,i}$ and $\bar{\lambda}_i$ is the isochoric material stretch in the Lagrangian direction $\mathbf{a}_{0,i}$ (here $\otimes$ is the dyadic tensor product).

Following Watton et al. (2004), we define a recruitment stretch variable $\bar{\lambda}_{r,i} > 1$, which may adapt to changes in the mechanical environment and is used to determine the stretch at which collagen fibres start to bear load. Working in terms of invariants, the square of the stretch in the collagen fibre, $\bar{I}_{4c,i} = \bar{\lambda}_{c,i}^2$, is written as

$$\bar{I}_{4c,i} = \begin{cases} 1 & \text{if } \bar{I}_{4,i} < \bar{I}_{4r,i} \\ \bar{I}_{4,i}/\bar{I}_{4r,i} & \text{else} \end{cases} \tag{2}$$

where $\bar{I}_{4r,i} = \bar{\lambda}_{r,i}^2 > 1$. From (2), it is clear that we do not model the stretch of collagen until the material in the fibre direction is stretched to a value above that of the collagen recruitment stretch.

Material deposition/degradation that occurs during G&R may also be associated with an increase or a decrease in total volume of the tissue. These volumetric changes, described by $\hat{v}$, will update the natural reference configuration, Ω_0, to an intermediate configuration, Ω, as seen in Fig. 1.

From Ω, it is not possible to return to Ω_0 without first reversing the volumetric changes via further growth/atrophy, i.e. Ω may be considered to be an updated reference configuration. The volumetric changes, $\hat{v}$, that occur during deposition/degradation of the constituents are later described in detail in Section 2.5.

2.2. Specific forms of strain-energy functions

A strain-energy density function is now introduced, suitable for arterial tissue, which for each constituent ζ incorporates a normalised density variable, $\hat{\rho}_\zeta = \rho_\zeta(\tau)/\rho_\zeta(\tau_0)$, where τ_0 is an initial time (before G&R) and τ is the current time, so that $\hat{\rho}_\zeta = 1$ at τ_0. The evolution of this density variable is further explored in Section 2.5. The strain-energy density is defined relative to unit reference volume. Due to the long time scale used for G&R (in months/years), needed for the mass evolution in arteries, we assume mass only originates as sources (or sinks) and neglect any mass flux across boundaries. For simplicity, we use the above-mentioned ratio of the current to reference density in the growth formulation, compared to, e.g., Epstein and Maugin (2000), Lubarda and Hoger (2002), Schmid et al. (2012). We outline the formulation shown by Watton et al. (2004) and express it in terms of invariants, but neglect the dependence on $\bar{I}_2$ and $\bar{I}_{5i}$ (see, e.g., Holzapfel et al., 2000). We
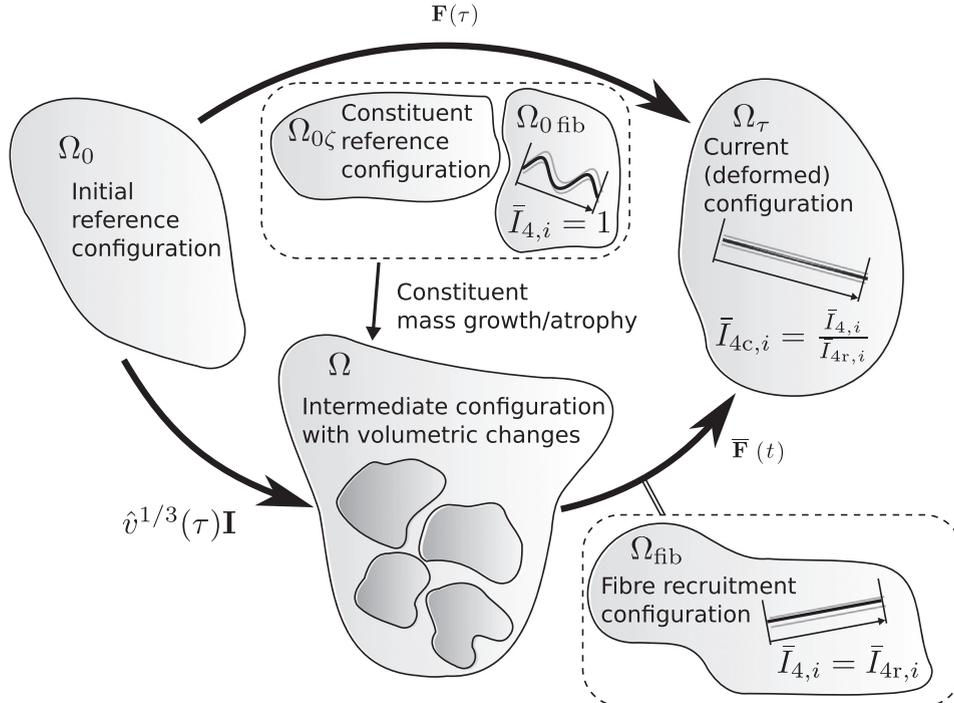
Fig. 1. Kinematics of VGR of a soft-tissue composed of multiple constituents. The local masses of constituents in the initial reference configuration, Ω_0, can adapt. Incompressibility of soft-tissue implies that there will be a volumetric change associated with changes in mass; this is depicted by the intermediate configuration Ω. The total deformation, $\mathbf{F}(\tau)$, to Ω_τ is therefore composed of the isochoric deformation, $\overline{\mathbf{F}}(t)$, from an intermediate configuration and of the volumetric changes, $\hat{v}^{1/3}(\tau)\mathbf{I}$, that lead to this intermediate configuration. Note that collagen fibres are configured to the arterial wall in a state of stretch in Ω_τ. This implies that they have an inherent waviness in the configuration, $\Omega_{0\,\text{fib}}$ and are on the onset of load bearing in the fibre recruitment configuration Ω_{fib}.

assume that the artery consists of two layers, the media (M) and the adventitia (A). We denote these layers $\gamma = \{M, A\}$. Each layer consists of an isotropic ground matrix (g) and contains two collagen fibre families (c, i), i.e. $i = \{1, 2\}$. In addition, the media layer consists of elastin fibres (e) which have evenly distributed fibre orientations and is, therefore, considered to have an isotropic contribution. In summary, the media has four constituents, $\zeta^M = \{e, g, c_1, c_2\}$ while the adventitia has three constituents, $\zeta^A = \{g, c_1, c_2\}$. The strain-energy function for the artery has a volumetric and an isochoric term, i.e.

$$\Psi = U(J, \hat{v}) + \overline{\Psi}^\gamma, \tag{3}$$

where the isochoric term, relating to the layers $\gamma = \{M, A\}$, is written as

$$\overline{\Psi}^\gamma = H(\gamma)\hat{\rho}_e\overline{\Psi}_e(\bar{I}_1) + \hat{\rho}_g^\gamma\overline{\Psi}_g(\bar{I}_1) + \sum_{i=1,2} \hat{\rho}_{c,i}^\gamma\overline{\Psi}_{c,i}^\gamma(\bar{I}_{4c,i}), \tag{4}$$

and where a Heaviside function is used to include the elastin constituent in the media, i.e.

$$H(\gamma) = \begin{cases} 0 & \text{if } \gamma = A, \\ 1 & \text{if } \gamma = M. \end{cases} \tag{5}$$

Note that we separate the strain energy function into a purely volumetric and a purely deviatoric part. This gives us the physiological response that volumetric changes (originating from adding/removing material) do not influence, e.g., the stretch felt by the collagen fibres. The fibres only 'feel' the deviatoric stretches. The same reasoning also applies to the isotropic matrix material.

For the ground matrix and the elastin we use a modified Neo-Hookean model for the isochoric and isotropic strain-energy functions, i.e.

$$\overline{\Psi}_g = \frac{\mu_g}{2}(\bar{I}_1 - 3), \quad \text{and} \quad \overline{\Psi}_e = \frac{\mu_e}{2}(\bar{I}_1 - 3), \tag{6}$$

where μ_g and μ_e are material parameters related to the shear modulus of an isotropic material. The collagen fibre family in the Lagrangian direction $\mathbf{a}_{0i}$ is modelled using

$$\overline{\Psi}_{c,i}^\gamma = \frac{k_1^\gamma}{2k_2^\gamma}\{\exp[k_2^\gamma(\bar{I}_{4c,i} - 1)^2] - 1\} \tag{7}$$

where $k_1^\gamma > 0$ and $k_2^\gamma > 0$ are material parameters for collagen. Note that using Eq. (2), and with the condition $\bar{I}_{4r} > 1$, it follows that $\bar{I}_{4c,i} \geq 1$ always by design, and hence the formulation (7) always fulfil convexity and ellipticity requirements (see Holzapfel and Ogden, 2009 for a discussion on convexity and ellipticity for this type of model).

2.3. Volumetric function

On a short time scale, t, arterial tissues may be considered nearly incompressible. Over longer time, however, the tissue may change its volume due to increases or decreases in mass. This volume change is later outlined in Sections 2.5.1–2.5.4 and described as the normalised volume change $\hat{v}(\tau)$ at time τ (see Eqs. (18), (21) or (23) in subsequent sections for their explicit expressions).

Similar to, e.g., Schmid et al. (2012) and Valentín et al. (2013), we may use this normalised volume change to govern the volumetric function, $U(J, \hat{v})$, according to

$$U(J, \hat{v}) = \frac{\mu_\kappa}{2}[J(t) - \hat{v}(\tau)]^2, \tag{8}$$

where the dependence on t and τ is shown explicitly for clarity. Here, μ_κ serves as a user specified penalty parameter enforcing the volume change as $J(t) \to \hat{v}(\tau)$. Note that this volume change is isotropic and has no directional dependence.

2.4. Stress tensors

Using the chain rule of differential calculus on (3), together with (5), the second Piola–Kirchhoff stress tensor $\mathbf{S} = 2\partial\Psi/\partial\mathbf{C}$ is given by

$$\mathbf{S} = Jp_h\mathbf{C}^{-1} + 2J^{-2/3}[H(\gamma)\hat{\rho}_e\overline{\psi}_{1e} + \hat{\rho}_g\overline{\psi}_{1\,g}]\text{Dev}(\,)\mathbf{I} + \sum_{i=1,2} \hat{\rho}_{c,i}^\gamma\overline{\psi}_{4c,i}^\gamma\bar{I}_{4r,i}^{-1}\text{Dev}(\mathbf{A}_{0,i}), \tag{9}$$

for $\gamma = M, A$, where $\text{Dev}(\bullet) = (\bullet) - (1/3)[\bullet : \mathbf{C}]\mathbf{C}^{-1}$ is the material deviatoric operator. Using (6) and (7), we have introduced the definitions

$$\overline{\psi}_{1j} \equiv \frac{\partial\overline{\Psi}_j}{\partial\bar{I}_1} = \frac{\mu_j}{2}, \quad j = g, e, \tag{10}$$

$$\overline{\psi}_{4c,i}^\gamma \equiv \frac{\partial\overline{\Psi}_{c,i}^\gamma}{\partial\bar{I}_{4c,i}} = k_1^\gamma(\bar{I}_{4c,i} - 1)\exp\left[k_2^\gamma(\bar{I}_{4c,i} - 1)^2\right], \tag{11}$$
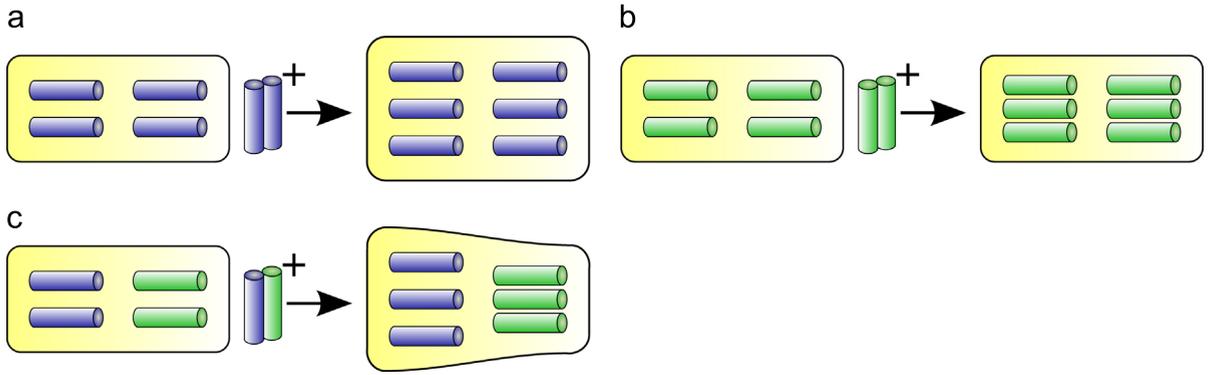
Fig. 2. Local mass changes are modelled through (a) constant individual density (CID), (b) adaptive individual density (AID), and (c) a mixture of CID and AID. The local loss of mass of a constituent leads to a reduced volume for CID and a reduced density for AID in an analogue way.

where we notice that $\overline{\psi}^{\gamma}_{4c,i} = 0$ for $\overline{I}_{4,i} < \overline{I}_{4r,i}$, as seen from (2). Using (8), we further get $p_h = \partial U / \partial J$ as

$$p_h = \mu_\kappa [J(t) - \hat{v}(\tau)]. \qquad (12)$$

The spatial version of the stress tensor is retrieved using a push-forward operation (Marsden and Hughes, 1994) of (9) to the Cauchy stress tensor, $\boldsymbol{\sigma}$, by $\boldsymbol{\sigma} = J^{-1} \mathbf{F} \mathbf{S} \mathbf{F}^\mathrm{T}$, i.e.

$$\boldsymbol{\sigma} = p_h \mathbf{I} + 2J^{-1} \sum_{\gamma = \mathrm{M,A}} \{[H(\gamma)\hat{\rho}_e \overline{\psi}_{1e} + \hat{\rho}_g \overline{\psi}_{1g}] \mathrm{dev}(\overline{\mathbf{b}}) + \sum_{i=1,2} \hat{\rho}^\gamma_{c,i} \overline{\psi}^\gamma_{4c,i} \overline{I}^{-1}_{4r,i} \mathrm{dev}(\overline{\mathbf{A}}_i)\}, \qquad (13)$$

where the spatial tensor $\overline{\mathbf{A}}_i = \overline{\mathbf{F}} \mathbf{a}_{0,i} \otimes \overline{\mathbf{F}} \mathbf{a}_{0,i} = \overline{\mathbf{a}}_i \otimes \overline{\mathbf{a}}_i$ is introduced and $\mathrm{dev}(\bullet) = (\bullet) - (1/3)[\bullet : \mathbf{I}]\mathbf{I}$ is the spatial deviatoric operator. The explicit expressions of the Lagrangian and the Eulerian elasticity tensors are given in Appendix A.

2.5. Growth, remodelling and volumetric adaptation

When modelling arterial VGR, it is essential to define rules for *how* and *when* mass changes occur within the artery. We, therefore, set the definitions for the assumptions on mass density and volume changes in Section 2.5.1. We then show the two underlying assumptions of mass growth namely through constant individual density (CID), through adaptive individual density (AID) and a mixture of the two assumptions in Sections 2.5.2, 2.5.3 and 2.5.4, respectively. In Section 2.5.5, we show the formulation for how growth can occur as a consequence of changes in the masses of individual constituents. The time evolution of the growth constituents is then shown in Section 2.5.6.

2.5.1. Mass, density and volume

A local mass change will result in alterations in either the density, the volume or both. We therefore need a formulation for how mass, density and volume are related for a tissue composed of multiple constituents. As shown by Schmid et al. (2012), using the infinitesimal mass dm, the infinitesimal volume dV and the density $\rho = dm/dV$, we introduce the normalised mass change, where τ_0 is the initial time (before G&R) and τ is the current time, as

$$\hat{m}(\mathbf{x}, \tau) = \frac{dm(\mathbf{x}, \tau)}{dm(\mathbf{x}, \tau_0)} = \frac{\rho(\mathbf{x}, \tau) dV(\mathbf{x}, \tau)}{\rho(\mathbf{x}, \tau_0) dV(\mathbf{x}, \tau_0)} = \hat{\rho}(\mathbf{x}, \tau) \hat{v}(\mathbf{x}, \tau), \qquad (14)$$

where we have used the normalised density change $\hat{\rho}(\mathbf{x}, \tau) = \rho(\mathbf{x}, \tau) / \rho(\mathbf{x}, \tau_0)$ and the normalised volume change $\hat{v}(\mathbf{x}, \tau) = dV(\mathbf{x}, \tau) / dV(\mathbf{x}, \tau_0)$. Here, $\mathbf{x}$ is the position vector in the deformed configuration. For a material with $\zeta = 1, ..., N$ constituents, the partial density, $\rho_\zeta(\mathbf{x}, \tau)$, and the individual density, $\varrho_\zeta(\mathbf{x}, \tau)$, of constituent ζ are defined as

$$\rho_\zeta(\mathbf{x}, \tau) = \frac{dm_\zeta(\mathbf{x}, \tau)}{dV(\mathbf{x}, \tau)}, \quad \text{and} \quad \varrho_\zeta(\mathbf{x}, \tau) = \frac{dm_\zeta(\mathbf{x}, \tau)}{dV_\zeta(\mathbf{x}, \tau)}, \qquad (15)$$

where $dm_\zeta(\mathbf{x}, \tau)$ is the partial mass of constituent ζ, $dV(\mathbf{x}, \tau)$ is the total volume and $dV_\zeta(\mathbf{x}, \tau)$ is the partial volume of constituent ζ. The volume fraction, $\phi_\zeta(\mathbf{x}, \tau)$, of constituent ζ is

$$\phi_\zeta(\mathbf{x}, \tau) = \frac{dV_\zeta(\mathbf{x}, \tau)}{dV(\mathbf{x}, \tau)}, \qquad (16)$$

which gives the relation $\rho_\zeta(\mathbf{x}, \tau) = \phi_\zeta(\mathbf{x}, \tau) \varrho_\zeta(\mathbf{x}, \tau)$. To clarify the notation, we have up until now explicitly stated the spatial and temporal dependence on the growth variables. In the following the spatial dependence will be dropped for visual clarity.

We assume that a mass change of a constituent results in either a volume change or a change in density for that constituent. This gives two possible scenarios: constant individual density (CID) where the individual density is constant

and the individual volume changes, or adaptive individual density (AID) where the individual density is adaptive and the individual volume is constant. These two assumptions are illustrated in Fig. 2(a) and (b).

Note that these scenarios are given in terms of the constituents. In a material with several constituents, such as arteries, we may have a mix where some constituents follow CID while others follow AID. For such a material the mixture will lead to an overall volume change as seen in Fig. 2(c). This leads to an altered partial density, ρ_ζ, which is a function of the total volume as given by (15)$_1$, despite the fact that the individual density, ϱ_ζ, of that same constituent remains constant.

2.5.2. Constant individual density (CID)

The relationship among mass, volume and density change is here given when assuming a constant individual density (Schmid et al., 2012), i.e. $\varrho_\zeta(\tau) = \varrho_\zeta(\tau_0)$, where the normalised mass change, $\hat{m}_\zeta$, and the normalised volume change, $\hat{v}_\zeta$, of constituent ζ are related according to

$$\hat{m}_\zeta(\tau) = \frac{dm_\zeta(\tau)}{dm_\zeta(\tau_0)} = \frac{\varrho_\zeta(\tau)dV_\zeta(\tau)}{\varrho_\zeta(\tau_0)dV_\zeta(\tau_0)} = \hat{\varrho}_\zeta(\tau)\hat{v}_\zeta(\tau) = \hat{v}_\zeta(\tau),$$ (17)

with $\hat{m}_\zeta(\tau_0) = 1, \forall \zeta$ and where $\hat{\varrho}_\zeta(\tau) = \varrho_\zeta(\tau)/\varrho_\zeta(\tau_0) = 1$ is the normalised individual density. The normalised tissue volume change $\hat{v}$ is then

$$\hat{v}(\tau) = \frac{dV(\tau)}{dV(\tau_0)} = \sum_{\zeta=1}^{N} \frac{dV_\zeta(\tau)}{dV(\tau_0)} = \sum_{\zeta=1}^{N} \frac{dV_\zeta(\tau)}{dV_\zeta(\tau_0)} \frac{dV_\zeta(\tau_0)}{dV(\tau_0)}$$
$$= \sum_{\zeta=1}^{N} \hat{v}_\zeta(\tau)\phi_\zeta(\tau_0) = \sum_{\zeta=1}^{N} \hat{m}_\zeta(\tau)\phi_\zeta(\tau_0),$$ (18)

and the normalised density is

$$\hat{\rho}_\zeta(\tau) = \frac{\rho_\zeta(\tau)}{\rho_\zeta(\tau_0)} = \frac{\varrho_\zeta(\tau)\phi_\zeta(\tau)}{\varrho_\zeta(\tau_0)\phi_\zeta(\tau_0)} = \frac{\phi_\zeta(\tau)}{\phi_\zeta(\tau_0)} = \frac{dV_\zeta(\tau)}{dV_\zeta(\tau_0)}\frac{dV(\tau_0)}{dV(\tau)}$$
$$= \hat{v}_\zeta(\tau)\frac{1}{\hat{v}(\tau)} = \hat{m}_\zeta(\tau)\frac{1}{\hat{v}(\tau)}.$$ (19)

2.5.3. Adaptive individual density (AID)

Instead of CID, we may assume that the individual density is adaptive leading to a constant individual volume, i.e. $dV_\zeta(\tau) = dV_\zeta(\tau_0)$. For AID, the normalised mass change now relates to the normalised individual density change according to

$$\hat{m}_\zeta(\tau) = \frac{dm_\zeta(\tau)}{dm_\zeta(\tau_0)} = \frac{\varrho_\zeta(\tau)dV_\zeta(\tau)}{\varrho_\zeta(\tau_0)dV_\zeta(\tau_0)} = \hat{\varrho}_\zeta(\tau)\hat{v}_\zeta(\tau) = \hat{\varrho}_\zeta(\tau),$$ (20)

where the normalised volume change of constituent ζ is $\hat{v}_\zeta(\tau) = 1$. Having constant individual volume in all constituents additionally leads to constant tissue volume, i.e.

$$\hat{v}(\tau) = \frac{dV(\tau)}{dV(\tau_0)} = \sum_{\zeta=1}^{N} \frac{dV_\zeta(\tau)}{dV(\tau_0)} = \sum_{\zeta=1}^{N} \frac{dV_\zeta(\tau)}{dV_\zeta(\tau_0)} \frac{dV_\zeta(\tau_0)}{dV(\tau_0)}$$
$$= \sum_{\zeta=1}^{N} \hat{v}_\zeta(\tau)\phi_\zeta(\tau_0) = \sum_{\zeta=1}^{N} \phi_\zeta(\tau_0) = 1.$$ (21)

The normalised density is now retrieved as

$$\hat{\rho}_\zeta(\tau) = \frac{\rho_\zeta(\tau)}{\rho_\zeta(\tau_0)} = \frac{\varrho_\zeta(\tau)\phi_\zeta(\tau)}{\varrho_\zeta(\tau_0)\phi_\zeta(\tau_0)} = \hat{\varrho}_\zeta(\tau)\frac{\phi_\zeta(\tau)}{\phi_\zeta(\tau_0)} = \hat{\varrho}_\zeta(\tau)\frac{dV_\zeta(\tau)}{dV_\zeta(\tau_0)}\frac{dV(\tau_0)}{dV(\tau)}$$
$$= \hat{\varrho}_\zeta(\tau)\frac{\hat{v}_\zeta(\tau)}{\hat{v}(\tau)} = \hat{m}_\zeta(\tau).$$ (22)

2.5.4. Mixed CID and AID

In tissues comprising multiple constituents, such as arteries, one may consider that some constituents follow the assumption of CID, while the other follows the assumption of AID. For example, one may assume that the mass change of collagen fibres in arteries occurs in a manner that makes it follow CID, while the mass change of elastin occurring during arterial diseases follows the assumption of AID (these assumptions are further discussed in Section 4.1).

For such a tissue, where some constituents follow CID while others follow AID, the normalised tissue volume becomes

$$\hat{v}(\tau) = \sum_{\zeta=1}^{N} \hat{v}_\zeta(\tau)\phi_\zeta(\tau_0) = \sum_{\zeta=1}^{N} \begin{cases} \hat{m}_\zeta(\tau)\phi_\zeta(\tau_0) & \text{when } \zeta \text{ follow CID} \\ \phi_\zeta(\tau_0) & \text{when } \zeta \text{ follow AID} \end{cases}$$ (23)

using (18) and (21), while using (19) or (22) the normalised density change is

$$\hat{\rho}_\zeta(\tau) = \hat{m}_\zeta(\tau)\frac{1}{\hat{v}(\tau)}. \tag{24}$$

2.5.5. Conservation of volume

As the individual volume is constant for materials following AID, if two constituents follow AID one may speculate that as matter is lost in one constituent, matter is increased in the other constituent that takes its place. This will be used later to relate the loss of elastin mass to an increase in the mass of the ground matrix. It can be modelled as an alteration of the individual density of the related constituents. With V^{AID} being the total volume of the materials following AID and $\sum_{\zeta=l,r}\phi_\zeta^{\mathrm{AID}}=1$ being the individual volume fraction of the materials following AID, where l and r stand for a constituent with lost and replaced material, respectively, we have the relation

$$V^{\mathrm{AID}}(\tau) = [\hat{\varrho}_l(\tau)\phi_l^{\mathrm{AID}}(\tau_0) + \hat{\varrho}_r(\tau)\phi_r^{\mathrm{AID}}(\tau_0)]V^{\mathrm{AID}}(\tau_0). \tag{25}$$

Using that $V^{\mathrm{AID}}(\tau) = V^{\mathrm{AID}}(\tau_0)$, this is reformulated as

$$\hat{\varrho}_r(\tau) = \left[1 - \hat{\varrho}_l(\tau)\phi_l^{\mathrm{AID}}(\tau_0)\right]\frac{1}{\phi_r^{\mathrm{AID}}(\tau_0)}, \tag{26}$$

which, according to (20), is used in (24) to retrieve the normalised density change of the replacement material.

2.5.6. Collagen remodelling

Collagen fibres are in a continual state of deposition and degradation and are configured to the arterial wall in the loaded configuration in a small state of stretch: we refer to this as the *attachment stretch* (Watton et al., 2004). A natural consequence is that the unloaded reference configurations of collagen constituents will remodel in response to changes to the geometrical configuration of the loaded artery. This can be simulated numerically by evolving the recruitment stretches, used in Eq. (2), i.e.

$$\frac{\partial\overline{\lambda}_{\mathrm{r},i}}{\partial\tau} = \alpha\frac{(\overline{I}_{4\mathrm{c},i} - \overline{I}_{4\mathrm{a},i})}{\overline{I}_{4\mathrm{a},i} - 1}, \tag{27}$$

where $\overline{I}_{4\mathrm{a},i} = \overline{\lambda}_{\mathrm{a},i}^2$ is related to the homeostatic collagen *attachment stretch* that acts as a material parameter and $\overline{I}_{4\mathrm{c},i} = \overline{I}_{4\mathrm{c},i}(\overline{\lambda}_{\mathrm{r},i})$ is given by Eq. (2). The parameter $\overline{\lambda}_{\mathrm{a},i}$ is the isochoric equivalent of the attachment stretch. The purpose of Eq. (27) is to get $\overline{I}_{4\mathrm{c},i} \to \overline{I}_{4\mathrm{a},i}$ in Eq. (2). The remodelling parameter α relates to the rate at which the collagen remodels. Using the explicit Euler method, where $\Delta\tau = \tau^{k+1} - \tau^k$, Eq. (27) is expressed as

$$\overline{\lambda}_{\mathrm{r},i}^{k+1} = \begin{cases} -\alpha\Delta\tau + \overline{\lambda}_{\mathrm{r},i}^k & \text{if } \overline{I}_{4,i}^k < \overline{I}_{4\mathrm{r},i}^k \\ \alpha\Delta\tau\dfrac{(\overline{I}_{4,i}^k/(\overline{\lambda}_{\mathrm{r},i}^k)^2 - \overline{I}_{4\mathrm{a},i})}{(\overline{I}_{4\mathrm{a},i} - 1)} + \overline{\lambda}_{\mathrm{r},i}^k & \text{else} \end{cases} \tag{28}$$

where the explicit expression from Eq. (2) shows the dependence on the recruitment stretch.

2.5.7. Collagen growth

In vascular homeostasis, the mass of the collagenous constituents is constant even though the fibers are in a continual state of deposition and degradation. However, in response to perturbations to the mechanical environment, vascular cells can respond by up (down)-regulating synthesis and down (up)-regulating degradation leading to a net increase (decrease) in mass. We outline the algorithm proposed to simulate this (Watton and Ventikos, 2009). The key assumptions of which are

- the reference configuration of the cells is equal to the reference configuration of the constituents that they are maintaining,
- the number of cells is proportional to the mass of constituents they are maintaining,
- in vascular homeostasis, the mass of the constituents is constant.

From these assumptions, the simplest (linear) differential equation for adapting the normalised mass of the collagenous constituents can be derived to be

$$\frac{\partial\hat{m}_{\mathrm{c},i}}{\partial\tau} = \beta\hat{m}_{\mathrm{c},i}\frac{(\overline{I}_{4\mathrm{c},i} - \overline{I}_{4\mathrm{a},i})}{\overline{I}_{4\mathrm{a},i} - 1}, \tag{29}$$

where the growth rate parameter β relates to the rate at which the mass of collagen can adapt.

2.5.8. Elastin degradation

The normalised mass ratio of elastin is used to prescribe the loss of elastin content in an artery, i.e. the atrophy of elastin, where it is a function of time and position:

$$\hat{m}_e = \hat{m}_e(\mathbf{X}, \tau). \tag{30}$$

The function in (30) varies depending on the case that is studied. We use a spatially homogeneous atrophy of the elastin in Section 3.1, and when modelling a AAA utilising the symmetry of a cylinder (see Section 3.2), we use

$$\hat{m}_e(x_3, \tau) = 1 - [1 - (\hat{m}_{e,min})^{\tau/\tau_{end}}]\exp[-\xi(x_3/l)^2], \tag{31}$$

where x_3 is the axial coordinate and where $\hat{m}_{e,min}$ is the minimum concentration of elastin at time $\tau = \tau_{end}$, $\xi \geq 0$ controls the axial width and shape of degradation and l is the length of the artery relative to a fixed Eulerian coordinate system.

In addition, we either assume that the (normalised) mass ratio of the ground matrix remains constant, i.e. $\hat{m}_g(\tau) = 1$, or that the normalised density of the ground matrix adapts in a direct response to the degradation of elastin according to (26) and (24). The motivation behind the alterations of the ground matrix density stems from the simplifying assumption that the ground matrix material takes the place of the degraded/fragmented elastin fibres. Details of this approach are further discussed in Section 4.1.

3. Representative numerical examples

The VGR formulation is implemented in the multi-purpose finite element analysis program FEAP (Taylor, 2011) by means of Eqs. (13) and (A.10) with their related equations, and all subsequent simulations use mixed $Q1/P0$ displacement/pressure finite elements that are based on the three-field Hu–Washizu variational approach (see, e.g., Simo and Taylor, 1991; Taylor, 2011; Holzapfel, 2003). Direction vectors, corresponding to the collagen fibre families, are implemented on the nodes and interpolated to the quadrature points using the element shape functions. For all examples shown below, it is observed that an increased mesh density does not yield any significant alteration in the results or the interpretation of the results.

3.1. Arterial segment

In an idealised model of an arterial segment, see Fig. 3, a quarter cylinder is constructed of two layers corresponding to the media and the adventitia, where the media is the innermost layer. Using dimensions corresponding to an (unloaded) abdominal aorta (Watton and Hill, 2009), the inner radius is $R_0 = 6.6$ mm and the thicknesses of the media and the adventitia are $H^M = 1.33$ mm and $H^A = 0.67$ mm, respectively. The fibres are oriented symmetrically in a tangent plane with an angle θ^γ between the circumferential axis and the fibre orientation. The angles for the media and adventitia are $\theta^M = \pm 30°$ and $\theta^A = \pm 60°$, respectively. For nodes located on the border between the media and the adventitia, the angles are linearly interpolated between θ^M and θ^A.

The axial length of the cylinder is 1 mm and the axial direction is pre-stretched to $\lambda_z = 1.3$. A follower type pressure load of $p = 120$ mmHg is applied to the innermost surface of the artery. The initial pressure and the axial stretch are applied
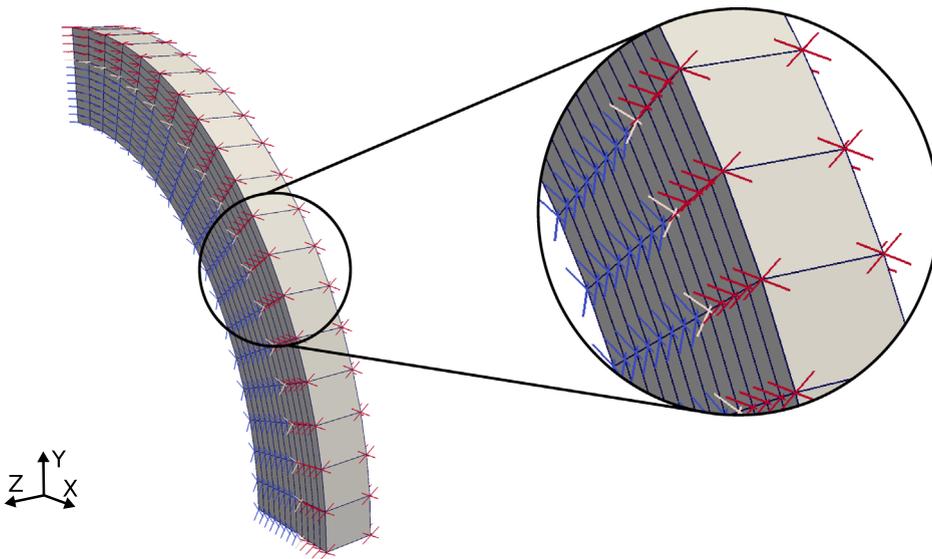
Fig. 3. FE model of the quarter cylinder in the initial reference state. The fibres are defined at the nodes and are shown as lines in blue and red on the nodes in the media and adventitia, respectively, and in white on the nodes at the border zone. (For interpretation of the references to colour in this figure caption, the reader is referred to the web version of this paper.)

Table 1

Material parameters, geometry and load for the artery. Parameters are in part adapted from Schmid et al. (2010) and Watton and Hill (2009) and in part to produce illustrative results.

Geometry		
Inner radius	R_0	6.6 mm
Wall thickness Media	H^M	1.33 mm
Wall thickness Adventitia	H^A	0.67 mm
Fibre angle		
Media	θ^M	$\pm 30°$
Adventitia	θ^A	$\pm 60°$
Load		
Pressure	p	120 mmHg (16 kPa)
Axial pre-stretch	λ_z	1.3
Material parameters		
Volumetric	μ_κ	100 MPa
Elastin	μ_e	133.8 kPa
Ground matrix	μ_g	$\mu_e/4 = 33.45$ kPa
Collagen Media	k_1^M	3.52 kPa
Collagen Adventitia	k_1^A	0.88 kPa
Exponential constant for collagen	$k_2^M = k_2^A$	40
Volume fractions		
Ground matrix	ϕ_g^γ	79%
Elastin	ϕ_e	6%
Collagen	$\phi_{c1}^\gamma + \phi_{c2}^\gamma$	$7.5 + 7.5 = 15\%$
Time constants		
Collagen remodelling	α	0.6 year^{-1}
Collagen growth	β	1.5 year^{-1}
Mass ratio of elastin at τ_{end}	$\hat{m}_{e,min}$	0.5
Time for degradation of elastin to $\hat{m}_{e,min}$	τ_{end}	10 years
Remodelling parameters		
Initial recruitment stretch	$\overline{\lambda}_{r0}(\mathbf{X}, \tau_0)$	1.13
Attachment parameter	$\overline{I}_{4a} = \overline{\lambda}_a^2$	1.195

incrementally in 10 equal load steps. The boundary conditions, where $\mathbf{u} = [u_x, u_y, u_z]^T$ are the nodal displacements in Cartesian coordinate X, Y, Z, are

$$
\begin{cases}
u_x(X = 0) = 0, \\
u_y(Y = 0) = 0, \\
u_z(Z = 0) = 0, \\
u_z(Z = 1 \text{ mm}) = 0.3 \text{ mm}, \\
p = 120 \text{ mmHg} \approx 16 \text{ kPa}.
\end{cases}
\tag{32}
$$

The mesh consists of 494 nodes and 216 hexahedral elements in total where the media and the adventitia have 8 and 4 elements transmurally, respectively, and both have 18 elements in the circumferential direction. In addition 18 quadrilateral elements are located on the inner surface on which the pressure acts.

The simulation is conducted in three consecutive steps:

Step 1: The initial time is set to $\tau = -2$ years and an initial load is applied where the pressure and the axial pre-stretch reach their final value in 10 iterations using $\Delta\tau = 0.1$ years. The values for p and λ_z are then held constant during subsequent steps. During this step the recruitment stretch, $\overline{\lambda}_r = \overline{\lambda}_{r0}$, is also constant.

Step 2: A homeostatic state is reached in 20 iterations using $\Delta\tau = 0.05$ years, where the collagen stretch equals the attachment stretch transmurally by allowing the recruitment stretch, $\overline{\lambda}_r$, to adapt using Eq. (27).

Step 3: The elastin degrades homogeneously using

$$
\hat{m}_e(X, \tau) = \hat{m}_e(X, \tau_0) \hat{m}_{e,min}^{\tau/\tau_{end}}, \quad \forall X^M
\tag{33}
$$

where $\hat{m}_{e,min} = 0.5$ is the normalised mass change of elastin that remains at time $\tau_{end} = 10$ years and $\hat{m}_e(X, \tau_0) = 1$, $\forall X^M$. Collagen remodels using Eq. (27) and grows using Eq. (29). The final time of $\tau_{end} = 10$ years is reached in 200 consecutive iterations with a constant size of $\Delta\tau = 0.05$ years.

Steps 1 and 2 occur before the artery grows and setting the time $\tau = -2$ years in step 1 ensures that $\tau_0 = 0^+$ at the start of Step 3. At time τ_0, the normalised mass concentrations are all $\hat{m}_g^\gamma(\tau_0) = \hat{m}_e(\tau_0) = \hat{m}_c^\gamma(\tau_0) = 1$.

3.1.1. Elastin only

Before including the collagen remodelling, we first consider a theoretical case where both layers consist of elastin only and observe the behaviour when this constituent is degraded in the artery.

The (normalised) mass ratio of elastin degrades according to (33) and the remaining material parameters, loads and dimensions are adapted from Schmid et al. (2010) and Watton and Hill (2009), and are summarised in Table 1, except the material parameter μ_e for elastin. In the absence of collagen we increase this material parameter in both layers to $\mu_e = 233.8$ kPa.

Letting elastin follow CID we see in Fig. 4(a) that the reduction of $\hat{m}_e$ leads to a reduced volume, $\hat{v}$, while for AID, the volume change, $\hat{v}$, remains constant. This is in accordance with Sections 2.5.2 and 2.5.3, where CID leads to volumetric changes while AID leads to constant volume. Note that for the CID case, the volume is reduced to half its original volume as the volume change follows the mass change according to (17). What occurs is perhaps counter-intuitive, but also reported by Valentín et al. (2013), is that when the elastin degradation is simulated via a reduction in volume (i.e. following CID) the arterial segment shrinks radially, as seen by the reduced inner radius, $\hat{r}_i$, in Fig. 4(b). This means that, when using CID, we get a reduction of the radius and not the expected enlargement, even though we have a reduction in elastin mass, i.e. $\hat{m}_e$ is reduced. This is distinct from what occurs when modelling elastin loss using AID, i.e. the radius increases.

3.1.2. Elastin and collagen

We now use the full two-layer composite model with both elastin and collagen fibres, where all material parameters are as listed in Table 1, and we explore three different scenarios:

- that collagen and elastin both follow AID (labelled AID–AID), which means that the individual volume is constant for both collagen and elastin as their masses change,
- that collagen and elastin both follow CID (labelled CID–CID), which means that the individual volume of collagen and elastin changes as their masses change,
- that collagen follows CID while elastin follows AID (labelled CID–AID), which means that the individual volume of collagen changes while the individual volume for elastin is constant as their masses change.

In addition, if elastin follows AID, the ground matrix also follows AID and takes the place of the degraded elastin. If elastin follows CID, however, the ground matrix remains in its homeostatic state and $\hat{m}_g(\tau) = \hat{m}_g(\tau_0)$. The motivation behind using CID or AID for collagen and elastin is discussed subsequently in Section 4.1.

We study the influences of these different approaches in order to determine the behaviour of the model with regard to simulating volumetric adaption. We compare deformation measures and adaptations in mass, density and volume. As seen in Fig. 5, the geometrical configuration for the different cases at time $\tau = \tau_{end}$ varies significantly. The greatest enlargement is seen for the assumption CID–AID and the smallest enlargement is seen for the assumption AID–AID. The nonlinear enlargement is also seen in Fig. 6(a) where the change of the normalised inner radius is shown over time. It is clear that CID–AID leads to an increase in inner radius which is almost 4 times that of the reference radius, while CID–CID leads to 2/3 of that enlargement. AID–AID leads to the smallest enlargement of about 1.5 times the reference radius. A similar trend is
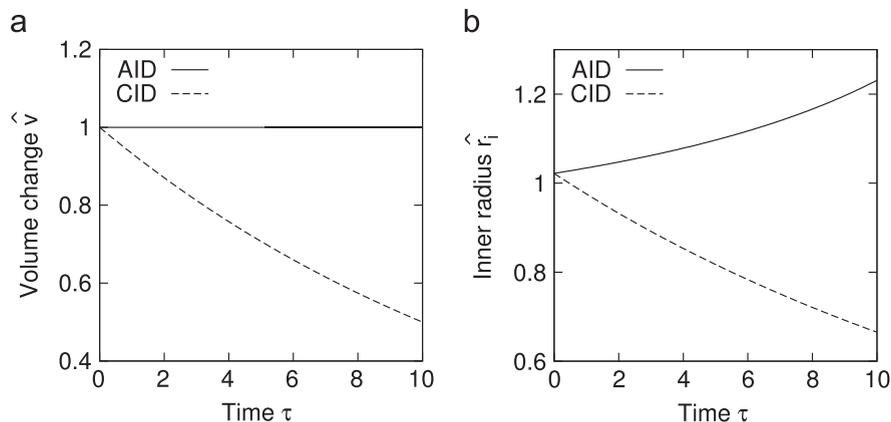
Fig. 4. Response to elastin degradation in a pressurised arterial segment with only the elastin component showing normalised volume change (left) and normalised inner radius (right). The values are normalised against the reference configuration at $\tau = -2$.
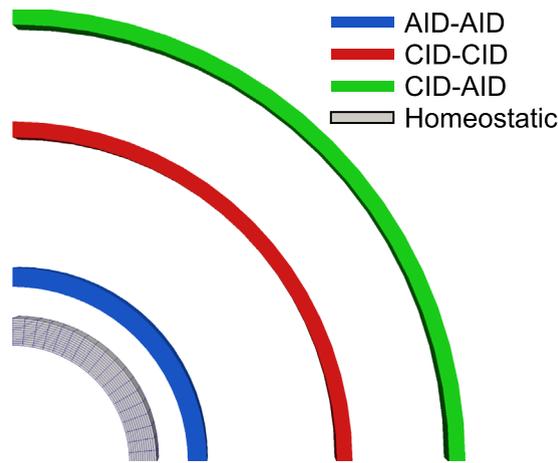
Fig. 5. Configuration of the artery at $\tau = \tau_{\mathrm{end}}$ under the different assumptions, AID–AID (blue), CID–CID (red) and CID–AID (green). The homeostatic configuration before elastin degradation starts is the same for all cases and is shown in grey. (For interpretation of the references to colour in this figure caption, the reader is referred to the web version of this paper.)
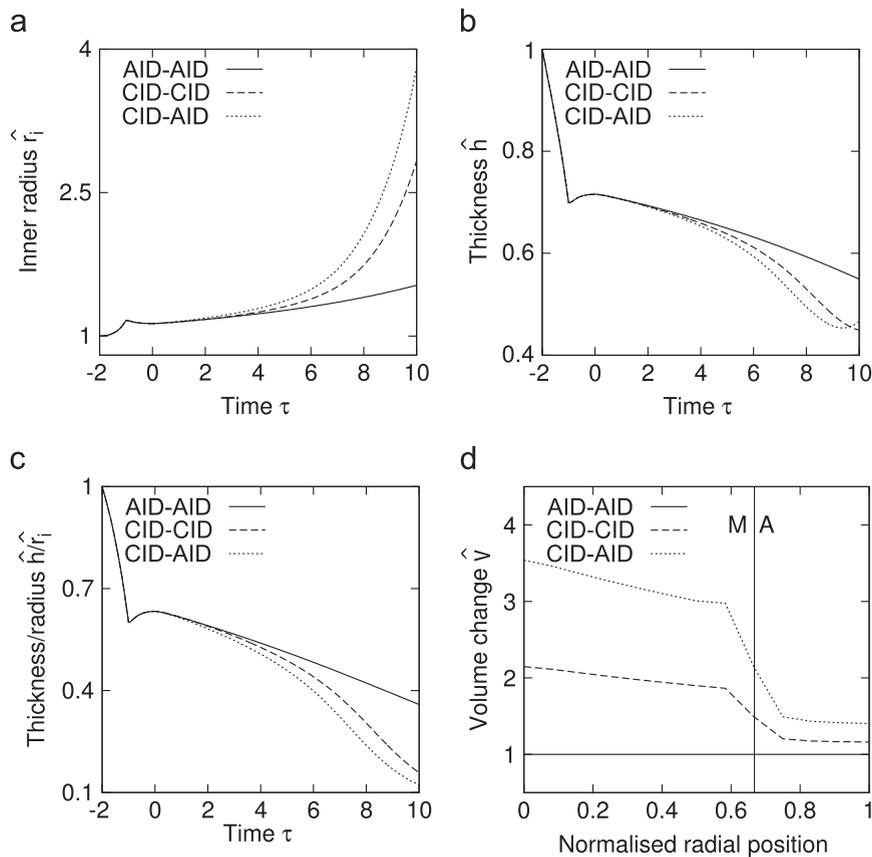
Fig. 6. Normalised changes in the inner radius, $\hat{r}_i$ (top left), and thickness, $\hat{h}$ (top right), where the values are normalised against the reference (undeformed) configuration. Ratio of thickness to inner radius (bottom left). Normalised volume change over the wall thickness, from inner to outer radius, at time $\tau = \tau_{\mathrm{end}}$ (bottom right). During load steps 1 and 2, preformed between time -2 and 0^-, a homeostatic configuration is reached.

also seen for the thickness over radius response, as seen in Fig. 6(c), where CID–AID leads to the lowest values and AID–AID to the largest.

When observing the normalised thickness $\hat{h}$ in Fig. 6(b), a different trend is seen. After a continuous decrease in thickness for CID–AID, due to the incompressible material being stretched circumferentially until about $\tau = 9$ years, a positive slope of thickness evolution is observed, despite the fact that the radius is continuously expanding. This increase in evolving

thickness, observed in Fig. 6(b), is a result of the change in volume of the material. The volume change at $\tau = \tau_{end}$ is shown in Fig. 6(d), transmurally through the arterial wall, where the values for $\hat{v}$ at the quadrature point have been projected to the nodes using the shape functions. As seen, the volume increase is largest for CID–AID, smaller for CID–CID, while non-existent for AID–AID. It is also evident that the volume change is largest at the innermost part of the arterial wall, i.e. in the media, while significantly lower in the adventitia.

Further transmural quantities are shown in Fig. 7, where the normalised mass and density changes, $\hat{m}$ and $\hat{\rho}$, have been projected from the quadrature points to the nodes using the shape functions. In the left column, the mass changes for the collagen, elastin and ground matrix are shown for cases AID–AID (top row), CID–CID (middle row) and CID–AID (bottom row), while in the right column, the density changes are shown for the same cases. Naturally, the mass and density changes are identical when the assumption AID–AID is used (top row) as this case is without volumetric changes, see Fig. 6(d). Notice, however, the increase in ground matrix mass and density, which is due to it replacing the loss of elastin. For the case
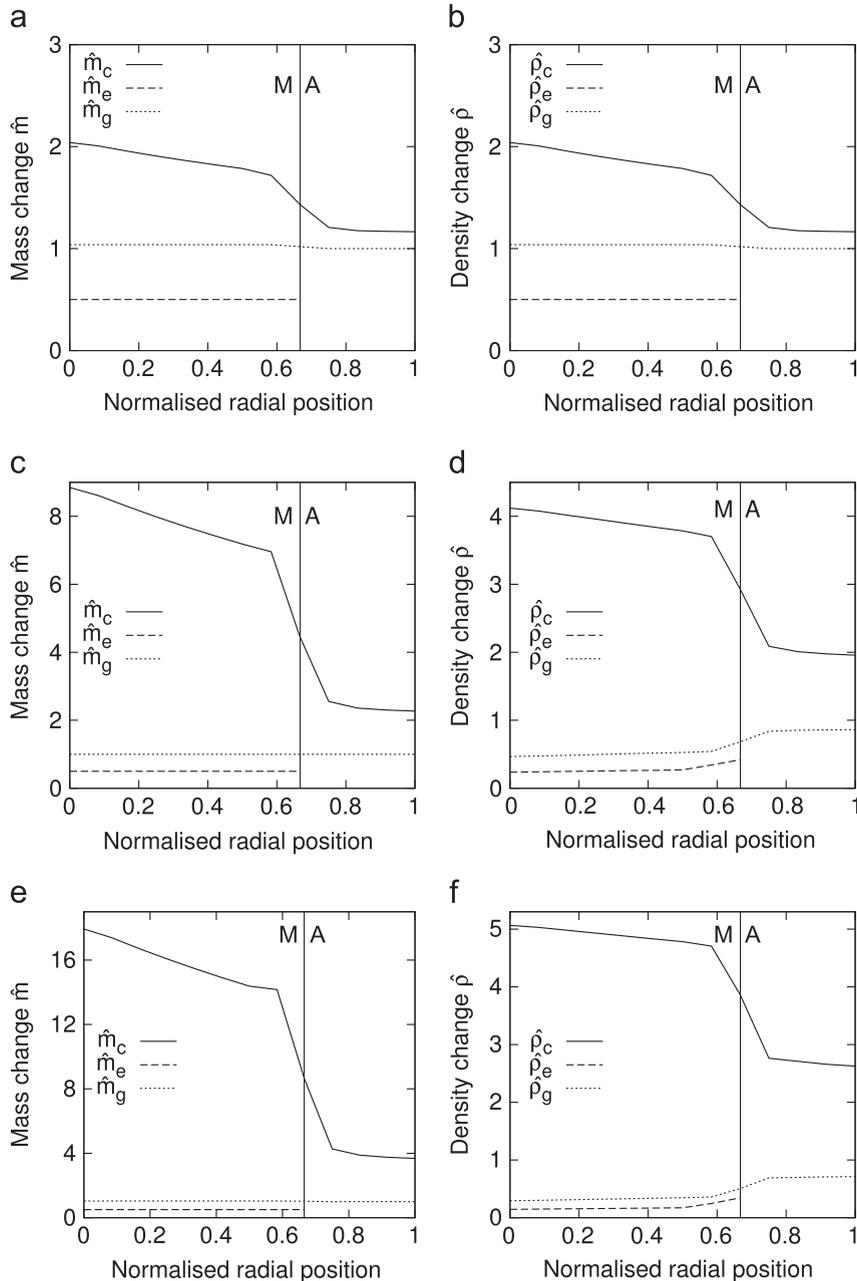
Fig. 7. Transmural changes in mass (left column) and density (right column) over the wall thickness, from inner to outer radius, at time $\tau = \tau_{end}$. Collagen and elastin follow AID–AID (top row), CID–CID (middle row) or CID–AID (bottom row).

of CID–CID (middle row) the mass change for collagen is more than the double than the density change for collagen at the border of the inner radius of the medial layer. For the case CID–AID (bottom row), the difference between the mass change and the density change for collagen, i.e. $\hat{m}_c$ and $\hat{\rho}_c$, is even more pronounced. For all cases, it is evident that the mass and density changes for collagen, i.e. $\hat{m}_c$ and $\hat{\rho}_c$, are significantly lower in the adventitia than in the media.

Notice also that the density changes, seen in Fig. 7(d) and (f), are reduced due to the volumetric changes seen in Fig. 6(d), according to (24). The normalised volumetric change for CID–CID and CID–AID is largest in the medial layer, which is why the normalised density change is lower there than in the adventitial layer.

3.2. AAA evolution

To illustrate the framework on a model of an idealised AAA, we apply the same simulation steps as outlined in Section 3.1 but let the atrophy of elastin follow Eq. (31) in Step 3. The Eulerian length of the artery is $l = L\lambda_z = 160$ mm, the parameter controlling the width of the degradation is $\xi = 20$ and all other material parameters are as listed in Table 1, except for $k_2^M = k_2^A = 52$. Due to the symmetry of the idealised artery, we only need to model 1/8 of a cylinder and the model consists of 2079 nodes and 1600 hexahedral elements with 4 elements transmurally, 10 elements circumferentially and 20 elements axially for both the media and the adventitia. In addition 200 quadrilateral elements are located on the inner surface on which the pressure acts. Similar boundary conditions and load protocol as in Section 3.1 are applied. The collagen follows the assumption of CID while the elastin follows the assumption of AID. The normalised individual density change of the ground matrix follows (26). The resulting normalised mass, density and volume changes are seen in Fig. 8. Again it is observed that the density changes for collagen are much lower than the mass changes. It is also clear that the largest volume increase occurs at the apex of the aneurysm which is also where the stretches are highest and where the increases of $\hat{m}_c$ and $\hat{\rho}_c$ are largest.

Similar to what was found in the previous example, see Fig. 7, the mass and density changes are larger in the medial layer than in the adventitia and the constituent density changes, shown in the right column, are given by the constituent mass changes, shown in the left column, divided by the total volume change, shown in Fig. 8(g); this in accordance with (24). Notice, however, that due to the initial volume fractions of the constituents, given in Table 1, the mass change of the ground matrix is very small compared to that of elastin and collagen.
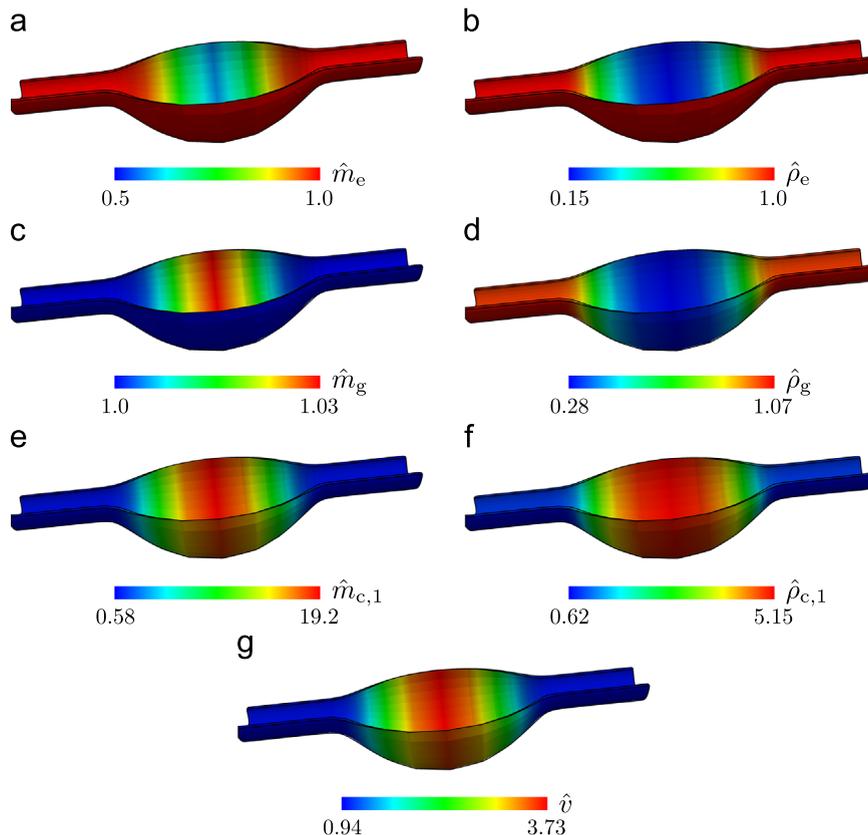
Fig. 8. Normalised mass, density and volume in a AAA at time $\tau = 10$ years using CID–AID for the collagen and elastin. For visual clarity, we show half of the artery by mirroring the simulated 1/8 artery.

4. Discussion

We have proposed a novel formulation for VGR of a fibre reinforced composite and detailed the equations needed for implementation of the framework in, e.g., a finite element setting. We investigated three scenarios for modelling the associated volumetric changes that accompany changes in mass of constituents: constant individual density (CID), adaptive individual density (AID) or a combination of the two (CID/AID). Whilst the proposed framework for modelling VGR in a thick walled fibre composite is generally at its core, we focused on its application to arterial G&R. We presented two illustrative applications of the modelling approach: firstly, VGR of an arterial segment under constant luminal pressure, and secondly, the evolution of an axi-symmetric AAA. These examples illustrated that the approach is suitable for modelling arterial G&R and volumetric adaption in a thick-walled setting. Moreover, they illustrated that the approach adopted to simulate volumetric adaption significantly influences the behaviour of the model. Note that the material and geometric parameters used are not chosen to produce realistic arterial VGR responses. Instead, they are chosen to produce illustrative results. Although not shown here, changing the parameters does not alter the conclusions reached through these examples, but alter only the visual clarity.

The examples show that the framework is suitable for modelling arterial VGR in a thick-walled setting. This is a major difference between, e.g., the models shown in Watton et al. (2004, 2011a), Gleason and Humphrey (2005) among others, where a membrane (or 2-D) formulation was used. Examining the different assumptions of constant density and/or volume showed that CID–AID led to larger displacements and a larger volume change, see Figs. 5 and 6. The end result of the normalised thickness evolution, $\hat{h}$, however, did not differ significantly, despite that the normalised inner radius, $\hat{r}_i$, was significantly larger in the CID–AID case compared to, especially, the AID–AID case. This can be attributed to the increased volume change, $\hat{v}$, seen in Fig. 6(d). Although not shown in Fig. 6(b), given enough time the slope of $\hat{h}$ for CID–CID would also be positive due to the volumetric expansion, similar to the CID–AID case. The AID–AID case, however, will never yield a positive slope of $\hat{h}$. Through Eqs. (21) and (22), and Figs. 6 and 4, it is obvious that using the assumption of AID for collagen and elastin yields a case without VGR. This case is in fact a direct extension of the membrane model, proposed by Watton et al. (2004), to a thick-walled formulation. Utilising the assumptions of CID for collagen (and/or elastin) further extends this formulation to include VGR and we make the general observation that including volumetric changes, as in the cases CID–CID and CID–AID, significantly altered the mechanical response compared to the case without volumetric changes, i.e. AID–AID.

4.1. Biological motivation behind CID or AID

If the local mass of constituents changes then either the density or the volume of the constituents (or both) must change. The biological motivation underlying CID is that as mass changes, the density is constant while the volume expands or shrinks. However, when using CID to model elastin degradation (for a theoretical model of the artery that consists only of elastin) a reduction of elastin mass leads to a decrease in the radius of the artery (see Fig. 4). This appears counter-intuitive, i.e. the weakening of the wall due to the reduction (or fragmentation) of elastin is often associated with aneurysmal enlargement. The reason why this occurs is subtle. The enforced volumetric change (associated with the mass decrease) implicitly changes the natural reference configuration of the elastin fibres, i.e. the geometrical configuration with which the stretches of the elastin are defined with respect to and consequently the artery shrinks in size. Hence we suggest that careful usage of the term *volumetric growth* is needed as in addition to *growth* it implicitly implies *remodelling*.

The question thus arises as to whether the CID approach to model volumetric adaption of the tissue in response to changes in the mass of elastin is physiologically justifiable. Elastin is a stable protein with a long half life (Alberts et al., 1994), which means that the rate of remodelling is very slow. Hence it is therefore reasonable to assume that during elastin atrophy, or elastin fragmentation, of a mature artery the remaining elastin fibrils maintain their structure and position, thus their reference configurations should not change as elastin is lost. Hence, for a mature artery, it may not be appropriate to model elastin degradation via CID which causes changes to the reference configuration. In fact, experimentally, it is observed that the degraded elastin fibrils are instead replaced by proteoglycans and connective tissue (Kornet et al., 2004). Furthermore, it has been shown in skin that areas of fragmented elastin fibres experience an increase in the formation of proteoglycans and connective tissue (Schlatmann and Becker, 1977; Campa et al., 1987). We therefore hypothesise that the individual volume of elastin remains the same, and that the reduction in elastin mass is replaced by an increase in the mass of proteoglycans and other connective tissues (which we here model as the remaining ground matrix). We suggest that for simulating the evolution of vascular diseases where elastin is lost, a sensible approach may be to model arterial VGR using the CID approach for collagen, AID for elastin and the ground matrix and add the constraint that the mass change for the ground matrix replaces the loss of mass of elastin, i.e. using (26) with both elastin and the remaining ground matrix following AID. This approach was illustrated for the evolution of a AAA in Fig. 8. Note that collagen can continually remodel its reference configuration as a natural consequence of the continual process of fibre deposition and degradation. Hence the implicit *remodelling* that occurs as a consequence of simulating volumetric adaption is consistent with collagen biology and CID is thus appropriate for collagen.

In this paper, we only consider growth of material components by either CID or AID. However, growth may be a consequence of simultaneous changes in density and volume. A further limitation is the use of an isotropic volumetric function, as biological tissues may not change volume isotropically, but instead have preferred orientations for volumetric

adaption. However, the limited amount of experimental data available currently motivates the use of isotropic volumetric functions. These limitations clearly illustrate the need for improved understanding of the biology of growth of soft living tissues through quantitative experiments. Such experiments will undoubtedly prove to be essential to guide the modelling community working on VGR of arteries and soft tissues in general.

We prescribed the degradation of elastin. However, the structural model can easily be integrated into a Fluid–Solid-Growth computational framework (Watton et al., 2009, 2011a,b) which will enable VGR to be linked to haemodynamic stimuli utilising patient-specific geometries (Aparício et al., 2014). Growth was linked to stretch-based evolution laws. However, the ability to accurately model volumetric changes as a consequence of G&R will enable changes to the arterial wall thickness to be predicted. This will be important if stress-based growth laws are utilised in the future. Moreover the model will enable for more sophisticated models of aneurysm evolution, e.g., simulating the destruction of the medial layer that occurs during intracranial aneurysm evolution and the thickening of the wall that occurs during AAA evolution.

5. Conclusions

We have proposed a novel formulation for volumetric G&R (VGR) of a fibre reinforced composite and detailed the equations needed for implementation of the framework in, e.g., a finite element setting. We investigated three scenarios for modelling the associated volumetric changes that accompany changes in mass of constituents: constant individual density (CID), adaptive individual density (AID) or a combination of the two (CID/AID). Using informative examples, such as VGR in an arterial segment under constant pressure, and simulation of evolution of an abdominal aortic aneurysm, we have shown that the choice of modelling approach significantly influences the predicted evolution, e.g., enlargement rates. In fact, we conclude that for modelling the evolution of vascular diseases where elastin degradation/fragmentation plays an important role, it may be preferable to utilise the assumption of CID for collagen and the assumption of AID for elastin and the ground matrix.

Acknowledgements

Appendix A. Lagrangian and Eulerian elasticity tensors

A.1. The Lagrangian elasticity tensor

Using (9) and (5), the elasticity tensor is calculated as

$$\mathbb{C} = 2\frac{\partial \mathbf{S}}{\partial \mathbf{C}} = \mathbb{C}_{\text{vol}} + H(\gamma)\mathbb{C}_{\text{e}} + \mathbb{C}_{\text{g}} + \sum_{i=1,2} \mathbb{C}_{\text{c},i}^{\gamma}, \quad \gamma \in \{M, A\}, \tag{A.1}$$

where $\mathbb{C}_{\text{vol}}$, $\mathbb{C}_{\text{e}}$, $\mathbb{C}_{\text{g}}$ and $\mathbb{C}_{\text{c},i}^{\gamma}$ pertains to the volumetric, elastin, ground matrix and collagen fibre terms, respectively. These terms are given by

$$\mathbb{C}_{\text{vol}} = 2\frac{\partial(Jp_{\text{h}}\mathbf{C}^{-1})}{\partial \mathbf{C}} = J\tilde{p}_{\text{h}}\mathbf{C}^{-1} \otimes \mathbf{C}^{-1} - 2Jp_{\text{h}}\mathbf{C}^{-1} \odot \mathbf{C}^{-1}, \tag{A.2}$$

$$\mathbb{C}_{j} = 4\frac{\partial}{\partial \mathbf{C}}\left(\hat{\rho}_{j}\overline{\psi}_{1j}\frac{\partial \overline{I}_{1}}{\partial \mathbf{C}}\right) = 4\hat{\rho}_{j}\left(\overline{\psi}_{11j}\frac{\partial \overline{I}_{1}}{\partial \mathbf{C}} \otimes \frac{\partial \overline{I}_{1}}{\partial \mathbf{C}} + \overline{\psi}_{1j}\frac{\partial^{2}\overline{I}_{1}}{\partial \mathbf{C}\partial \mathbf{C}}\right), \quad j = g, e \tag{A.3}$$

$$\mathbb{C}_{\text{c},i}^{\gamma} = 4\frac{\partial}{\partial \mathbf{C}}\left(\hat{\rho}_{\text{c},i}^{\gamma}\overline{\psi}_{4\text{c},i}^{\gamma}\frac{\partial \overline{I}_{4\text{c},i}}{\partial \mathbf{C}}\right) = 4\hat{\rho}_{\text{c},i}^{\gamma}\left(\overline{\psi}_{44\text{c},i}^{\gamma}\frac{\partial \overline{I}_{4\text{c},i}}{\partial \mathbf{C}} \otimes \frac{\partial \overline{I}_{4\text{c},i}}{\partial \mathbf{C}} + \overline{\psi}_{4\text{c},i}^{\gamma}\frac{\partial^{2}\overline{I}_{4\text{c},i}}{\partial \mathbf{C}\partial \mathbf{C}}\right), \tag{A.4}$$

where the definitions $\tilde{p}_{\text{h}} \equiv p_{\text{h}} + Jdp_{\text{h}}/dJ$, $\mathbf{C}^{-1} \odot \mathbf{C}^{-1} \equiv -\partial \mathbf{C}^{-1}/\partial \mathbf{C}$, $\overline{\psi}_{11j} \equiv \partial^{2}\overline{\Psi}_{j}/(\partial \overline{I}_{1}\partial \overline{I}_{1})$, $(j = g, e)$ and $\overline{\psi}_{44\text{c},i}^{\gamma} \equiv \partial^{2}\overline{\Psi}_{4\text{c},i}^{\gamma}/(\partial \overline{I}_{4\text{c},i}\partial \overline{I}_{4\text{c},i})$ are introduced. In $\tilde{p}_{\text{h}}$ we get the relation $dp_{\text{h}}/dJ = \mu_{\kappa}$ using (12). With the specific strain-energy functions (6) and (7) we get the expressions

$$\overline{\psi}_{11j} = 0, \quad j = g, e, \tag{A.5}$$

$$\overline{\psi}_{44\text{c},i}^{\gamma} = k_{1}^{\gamma}[1 + 2k_{2}^{\gamma}(\overline{I}_{4\text{c},i} - 1)^{2}\exp[k_{2}^{\gamma}(\overline{I}_{4\text{c},i} - 1)^{2}]. \tag{A.6}$$

For (A.3) and (A.4), we expand the derivatives and retrieve

$$\mathbb{C}_{j} = 4\hat{\rho}_{j}J^{-4/3}\underbrace{\overline{\psi}_{11j}}_{=0}\text{Dev }\mathbf{I} \otimes \text{Dev }\mathbf{I}$$

$$-\frac{4}{3}\hat{\rho}_j J^{-2/3}\overline{\psi}_{1\,j}(\mathbf{C}^{-1}\otimes\mathrm{Dev}\,\mathbf{I}+\mathrm{Dev}\,\mathbf{I}\otimes\mathbf{C}^{-1}-I_1\tilde{\mathbb{P}}),\quad j=\mathrm{g,e},\tag{A.7}$$

and

$$\begin{aligned}\mathbb{C}^{\gamma}_{\mathrm{c},i}&=4\hat{\rho}^{\gamma}_{\mathrm{c},i}J^{-4/3}\overline{I}^{-2}_{4\mathrm{r}}\overline{\psi}^{\gamma}_{44\mathrm{c},i}\mathrm{Dev}\,\mathbf{A}_{0,i}\otimes\mathrm{Dev}\mathbf{A}_{0,i}\\&-\frac{4}{3}\hat{\rho}^{\gamma}_{\mathrm{c},i}J^{-2/3}\overline{I}^{-1}_{4\mathrm{r},i}\overline{\psi}^{\gamma}_{4\mathrm{c},i}[\mathbf{C}^{-1}\otimes\mathrm{Dev}\,\mathbf{A}_{0,i}+\mathrm{Dev}\,\mathbf{A}_{0,i}\otimes\mathbf{C}^{-1}-I_{4,i}\tilde{\mathbb{P}}],\end{aligned}\tag{A.8}$$

for $\overline{I}_{4,i}\geq\overline{I}_{4\mathrm{r},i}$ and $\mathbb{C}^{\gamma}_{\mathrm{c},i}=\mathbb{O}$ otherwise, where $\mathbb{O}$ is a fourth order tensor of zeros. Here

$$\tilde{\mathbb{P}}=\mathbf{C}^{-1}\odot\mathbf{C}^{-1}-\frac{1}{3}\mathbf{C}^{-1}\otimes\mathbf{C}^{-1}\tag{A.9}$$

is a modified fourth-order projection tensor (see, e.g., Holzapfel, 2000).

A.2. The Eulerian elasticity tensor

The elasticity tensor $\mathbb{c}$ in the Eulerian description is retrieved using the push-forward operation on $\mathbb{C}$, i.e. $[\mathbb{c}]_{abcd}=J^{-1}F_{aA}F_{bB}F_{cC}F_{dD}[\mathbb{C}]_{ABCD}$, so that

$$\mathbb{c}=\mathbb{c}_{\mathrm{vol}}+\sum_{\gamma=\mathrm{M,A}}[H(\gamma)\mathbb{c}_{\mathrm{e}}+\mathbb{c}_{\mathrm{g}}+\sum_{i=1,2}\mathbb{c}^{\gamma}_{\mathrm{c},i}],\tag{A.10}$$

which is the analogue of Eq. (A.1). Using (A.2), the volumetric elasticity tensor $\mathbb{c}_{\mathrm{vol}}$ in the Eulerian description is

$$\mathbb{c}_{\mathrm{vol}}=J(\tilde{p}_{\mathrm{h}}\mathbf{I}\otimes\mathbf{I}-2p_{\mathrm{h}}\mathbb{I}),\tag{A.11}$$

where $\mathbb{I}$ is the fourth-order spatial unit tensor. The spatial version of (A.7) and (A.8) is similarly

$$\mathbb{c}_j=4\hat{\rho}_j\underbrace{\overline{\psi}_{11\,j}}_{=\,0}\mathrm{dev}\,\overline{\mathbf{b}}\otimes\mathrm{dev}\,\overline{\mathbf{b}}-\frac{4}{3}\hat{\rho}_j\overline{\psi}_{1\,j}(\mathbf{I}\otimes\mathrm{dev}\,\overline{\mathbf{b}}+\mathrm{dev}\,\overline{\mathbf{b}}\otimes\mathbf{I}-\overline{I}_1\mathbb{P}),\quad j=\mathrm{g,e}.\tag{A.12}$$

and

$$\mathbb{c}^{\gamma}_{\mathrm{c},i}=4\hat{\rho}^{\gamma}_{\mathrm{c},i}\overline{I}^{-2}_{4\mathrm{r},i}\overline{\psi}^{\gamma}_{44\mathrm{c},i}\mathrm{dev}\,\overline{\mathbf{A}}_i\otimes\mathrm{dev}\,\overline{\mathbf{A}}_i-\frac{4}{3}\hat{\rho}^{\gamma}_{\mathrm{c},i}\overline{I}^{-1}_{4\mathrm{r},i}\overline{\psi}^{\gamma}_{4\mathrm{c},i}[\mathbf{I}\otimes\mathrm{dev}\,\overline{\mathbf{A}}_i+\mathrm{dev}\,\overline{\mathbf{A}}_i\otimes\mathbf{I}-\overline{I}_{4,i}\mathbb{P}],\tag{A.13}$$

for $\overline{I}_{4,i}\geq\overline{I}_{4\mathrm{r},i}$ and $\mathbb{c}^{\gamma}_{\mathrm{c},i}=\mathbb{O}$ otherwise, where $\mathbb{O}$ is a fourth order tensor of zeros. Here, we also use $\mathbb{P}=\mathbb{I}-\frac{1}{3}\mathbf{I}\otimes\mathbf{I}$.

References

Alberts, B., Bray, D., Lewis, J., Raff, M., Roberts, K., Watson, J.D., 1994. Molecular Biology of the Cell. Garland Publishing, New York.

Aparício, P., Mandaltsi, A., Boamah, J., Chen, H., Selimovic, A., Bratby, M., Uberoi, R., Ventikos, Y., Watton, P.N., 2014. Modelling the influence of endothelial heterogeneity on the progression of arterial disease: application to abdominal aortic aneurysm evolution. Int. J. Numer. Meth. Biomed. Eng. 30, 563–586.

Baek, S., Rajagopal, K.R., Humphrey, J.D., 2006. A theoretical model of enlarging intracranial fusiform aneurysms. J. Biomech. Eng. 128, 142–149.

Campa, J.S., Greenhalgh, R.M., Powell, J.T., 1987. Elastin degradation in abdominal aortic aneurysms. Atherosclerosis 65, 13–21.

Epstein, M., Maugin, G.A., 2000. Thermomechanics of volumetric growth in uniform bodies. Int. J. Plast. 16, 951–978.

Eriksson, T., Kroon, M., Holzapfel, G., 2009. Influence of medial collagen organization and axial in situ stretch on saccular cerebral aneurysm growth. J. Biomech. Eng. 131, 101010.

Flory, P.J., 1961. Thermodynamic relations for highly elastic materials. Trans. Faraday Soc. 57, 829–838.

Gleason, R.L., Humphrey, J.D., 2005. A 2D constrained mixture model for arterial adaptations to large changes in flow, pressure and axial stretch. Math. Med. Biol. 22, 347–369.

He, C.M., Roach, M.R., 1994. The composition and mechanical properties of abdominal aortic aneurysms. J. Vasc. Surg. 20, 6–13.

Holzapfel, G.A., 2000. Nonlinear Solid Mechanics. A Continuum Approach for Engineering. John Wiley & Sons, Chichester.

Holzapfel, G.A., 2003. Structural and numerical models for the (visco)elastic response of arterial walls with residual stresses. In: Holzapfel, G.A., Ogden, R.W. (Eds.), Biomechanics of Soft Tissue in Cardiovascular Systems, CISM Courses and Lectures, vol. 441. Springer-Verlag, Wien, New York.

Holzapfel, G.A., Gasser, T.C., Ogden, R.W., 2000. A new constitutive framework for arterial wall mechanics and a comparative study of material models. J. Elasticity 61, 1–48.

Holzapfel, G.A., Ogden, R.W., 2009. Constitutive modelling of passive myocardium: a structurally based framework for material characterization. Philos. Trans. R. Soc. A 367, 3445–3475.

Humphrey, J.D., Holzapfel, G.A., 2012. Mechanics, mechanobiology, and modeling of human abdominal aorta and aneurysms. J. Biomech. 45, 805–814.

Kornet, L., Bergen, A.A.B., Hoeks, A.P.G., Cleutjens, J.P., Oostra, R.J., Daemen, M.J., van Soest, S., Reneman, R.S., 2004. In patients with pseudoxanthoma elasticum a thicker and more elastic carotid artery is associated with elastin fragmentation and proteoglycans accumulation. Ultrasound Med. Biol. 30, 1041–1048.

Lubarda, V.A., Hoger, A., 2002. On the mechanics of solids with a growing mass. Int. J. Solids Struct. 39, 4627–4664.

Marsden, J.E., Hughes, T.J.R., 1994. Mathematical Foundations of Elasticity. Dover, New York.

Schlatmann, T.J., Becker, A.E., 1977. Histologic changes in the normal aging aorta: implications for dissecting aortic aneurysm. Am. J. Cardiol. 39, 13–20.

Schmid, H., Grytsan, A., Postan, E., Watton, P.N., Itskov, M., 2013. Influence of differing material properties in media and adventitia on arterial adaption: application to aneurysm formation and rupture. Comput. Methods Biomech. Biomed. Eng. 16, 33–53.

Schmid, H., Pauli, L., Paulus, A., Kuhl, E., Itskov, M., 2012. Consistent formulation of the growth process at the kinematic and constitutive level for soft tissues composed of multiple constituents. Comput. Methods Biomech. Biomed. Eng. 15, 547–561.

Schmid, H., Watton, P.N., Maurer, M.M., Wimmer, J., Winkler, P., Wang, Y.K., Röhrle, O., Itskov, M., 2010. Impact of transmural heterogeneities on arterial adaptation: application to aneurysm formation. Biomech. Model. Mechanobiol. 9, 295–315.

Simo, J.C., Taylor, R.L., 1991. Quasi-incompressible finite elasticity in principal stretches. Continuum basis and numerical algorithms. Comput. Methods Appl. Mech. Eng. 85, 273–310.

Taylor, R.L., 2011. FEAP – A Finite Element Analysis Program, Version 8.3 User Manual. University of California at Berkeley, Berkeley, CA.

Valentín, A., Humphrey, J.D., Holzapfel, G.A., 2011. A multi-layered computational model of coupled elastin degradation, vasoactive dysfunction, and collagenous stiffening in aortic aging. Ann. Biomed. Eng. 39, 2027–2045.

Valentín, A., Humphrey, J.D., Holzapfel, G.A., 2013. A finite element based constrained mixture implementation for arterial growth, remodeling, and adaptation: theory and numerical verification. Int. J. Numer. Methods Biomed. Eng. 29, 822–849.

Wagenseil, J.E., Mecham, R.P., 2009. Vascular extracellular matrix and arterial mechanics. Physiol. Rev. 89, 957–989.

Watton, P.N., Hill, N.A., 2009. Evolving mechanical properties of a model of abdominal aortic aneurysm. Biomech. Model. Mechanobiol. 8, 25–42.

Watton, P.N., Hill, N.A., Heil, M., 2004. A mathematical model for the growth of the abdominal aortic aneurysm. Biomech. Model. Mechanobiol. 3, 98–113.

Watton, P.N., Raberger, N.B., Holzapfel, G.A., Ventikos, Y., 2009. Coupling the hemodynamic environment to the evolution of cerebral aneurysms: computational framework and numerical examples. ASME J. Biomed. Eng. 131, 101003.

Watton, P.N., Ventikos, Y., 2009. Modelling evolution of saccular cerebral aneurysms. J. Strain Anal. 44, 375–389.

Watton, P.N., Selimovic, A., Raberger, N.B., Huang, P., Holzapfel, G.A., Ventikos, Y., 2011a. Modelling evolution and the evolving mechanical environment of saccular cerebral aneurysms. Biomech. Model. Mechanobiol. 10, 109–132.

Watton, P.N., Ventikos, Y., Holzapfel, G.A., 2011b. Modelling Cerebral Aneurysm Evolution, Biomechanics and Mechanobiology of Aneurysms. Springer-Verlag, Heidelberg.